10 Non-equilibrium and irreversible processes

10.1 INTRODUCTION AND PERSPECTIVE

In the preceding chapters of this book we have dealt extensively with equilibrium properties of a wide variety of models and materials. We have emphasized the importance of insuring that equilibrium has been reached, and we have discussed the manner in which the system may approach the correct distribution of states, i.e. behavior before it comes to equilibrium. This latter topic has been treated from the perspective of helping us understand the difficulties of achieving equilibrium. The theory of equilibrium behavior is well developed and in many cases there is extensive, reliable experimental information available.

In this chapter, however, we shall consider models which are inherently non-equilibrium. This tends to be rather uncharted territory. For some cases theory exists, but it has not been fully tested. In other situations there is essentially no theory to rely upon. In some instances the simulation has preceded the experiment and has really led the way in the development of the field. As in the earlier chapters, for pedagogical reasons we shall concentrate on relatively simple models, but the presentation can be generalized to more complex systems.

Some introductory material on related 'kinetic Monte Carlo' methods for processes close to equilibrium (diffusive separation kinetics, etc.) was already given in Section 4.4.3 and may serve as an introduction to the present chapter.

10.2 DRIVEN DIFFUSIVE SYSTEMS (DRIVEN LATTICE GASES)

Over two decades ago a deceptively simple modification of the Ising lattice gas model was introduced (Katz *et al.*, 1984) as part of an attempt to understand the behavior of superionic conductors. In this 'standard model' a simple Ising lattice gas Hamiltonian describes the equilibrium behavior of a system, i.e.

$$\mathcal{H} = -\mathcal{J} \sum_{\langle i,j \rangle} n_i n_j, \qquad n_i = 0, 1. \tag{10.1}$$

In equilibrium the transition rate from state X to state X', $W(X \to X') = w(\beta \Delta \mathcal{H})$, is some function which satisfies detailed balance (see Section 4.2).

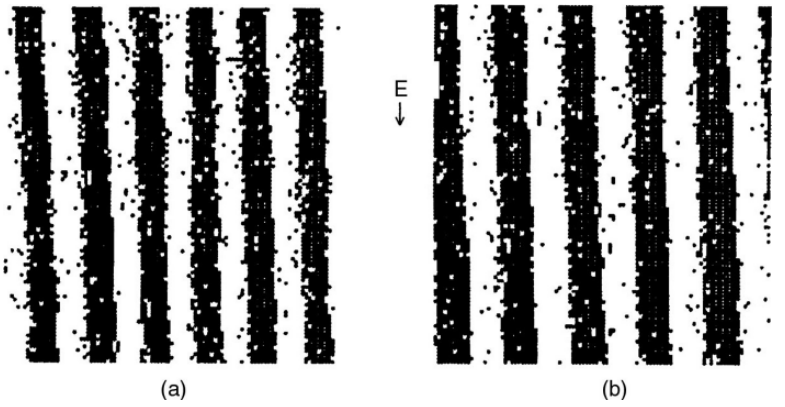

Fig. 10.1 Typical configurations for the 'standard model' driven diffusive lattice gas on a 100 × 100 lattice with a periodic boundary condition in the horizontal direction and a shifted periodic boundary condition in the vertical direction. The shift is given by h, where: (a) $h = 12$; (b) $h = 16$. From Schmittmann and Zia (1995).

A simple, uniform driving field **E** is applied in one direction of the lattice and 'spins' (or particle-hole pairs) are exchanged with a probability which is biased by this driving field. This process drives the system away from equilibrium regardless of which kinetic rule is used for the exchange, and the transition rate then becomes

$$W(X \to X') = w[(\Delta\mathcal{H} + lE)/k_{\mathrm{B}}T], \tag{10.2}$$

where $l = +1$, 0, or –1 is the distance the particle moved along **E**, and w is the same function used for the transition in the absence of the driving field. Periodic boundary conditions are applied and the system eventually reaches a non-equilibrium steady state in which a current then flows in the direction parallel to the driving field. These driven lattice gases are perhaps the simplest examples of NESS (non-equilibrium steady state) in which the Hamiltonian alone is *not* the governing feature of the resultant behavior. Since the number of particles (in lattice-gas language) is held fixed, the procedure is carried out at constant magnetization (in Ising model language) and spins are exchanged instead of flipped.

Patterns form and produce regions which are relatively free of particles and other regions which are quite densely occupied. As an example, in Fig. 10.1 we show the development of a pattern in a simple Ising model at fixed magnetization with a screw periodic boundary condition in the direction parallel to the driving field. Depending upon the magnitude of the shift in the boundary, different numbers of stripes appear in the steady state. Not only are 'snapshots' of the system generated, but the usual bulk properties are calculated as well. These may show indications of phase transitions just as they would in the case of equilibrium behavior. In addition to the bulk properties, the structure factor $S(\mathbf{k}, L)$ provides important information about the correlations. Indeed, phase transitions can be observed in these systems and peaks in the structure

factor offer convincing evidence of the transitions. Because the driving field distinguishes one direction from all others, the behavior is strongly anisotropic with the consequence that the usual scaling relations must be modified, so that for an infinite system

$$S(k_\perp, k_\parallel) = k_\perp^{-2+\eta} S_\perp \left(k_{||}/k_\perp^{1+\Delta}\right), \tag{10.3}$$

where Δ characterizes the anomalous dimension of the longitudinal momenta $k_\parallel$. Of course, modifications may be made in the nature of the interactions, the lattice size, and the aspect ratio of the system. At this time there is still some controversy about the values of the critical exponents in different models, and it is likely that the question of anisotropy will prove to be essential to the understanding of the behavior. In fact, a good framework for the understanding of Monte Carlo data (Wang, 1996) has been provided by an extension of finite size scaling which takes into account two different correlation length exponents, $\nu_\parallel$ and $\nu_\perp$, in the directions parallel and perpendicular to the flow, respectively (Binder and Wang, 1989; Leung, 1991).

Caracciolo *et al.* (2004) looked quite carefully at finite size scaling in the high temperature phase of the driven lattice gas system in an infinite driving field. Their results for the susceptibility and correlation length confirmed field theoretic predictions (Janssen and Schmittmann, 1986; Leung and Cardy, 1986), i.e. $\gamma_\perp = 1,\ \nu_\perp = 1/2$. Finite size scaling of the magnetization yielded $\beta_\perp/\nu_\perp = 1.023\,(43)$, in agreement with mean field predictions. Their data confirmed the importance of anisotropic finite size scaling and showed that the interplay between the time scale at which correlations are measured and finite size effects may complicate the analysis.

Despite this progress, the driven lattice gas is still to a large extent 'terra incognita' within the field of non-equilibrium statistical mechanics. This statement may be drawn from surprising results from two studies which we now briefly describe. First, a different study of the structure factor and probability distribution of the driven diffusive system confirmed violations of detailed balance and the breakdown of the 'decoupling' of stationary properties from the explicit dynamic rules for spin exchange (Kwak *et al.*, 2004). The secrets of these intriguing systems are slowly being uncovered through the combination of careful Monte Carlo simulations and theoretically based analyses. As a second example we draw the reader's attention to an interesting variation consisting of an Ising lattice gas driven to non-equilibrium steady states by being coupled to two thermal baths as introduced by Praestgaard *et al.* (2000). Monte Carlo methods were applied to a two-dimensional system in which one of the baths was fixed at infinite temperature. Both generic long range correlations in the disordered state and critical properties near the second order transition were measured, and anisotropic scaling was used to extract T_c and some critical exponents. On the theoretical front, a continuum theory, in the spirit of Landau–Ginzburg, was presented. The critical behavior of this system apparently belongs to a universality class which is quite different from the uniformly driven Ising model.

A recent comparison of several related interacting particle models that exhibit currents, e.g. lattice gases and Lennard–Jones systems with a biased hopping of particles which mimics features of traffic and anisotropic phase segregation in simple fluids and mixtures, enhances our understanding of non-equilibrium, anisotropic, particle flow (Marro, 2008).

Recently, interesting attempts were made to realize the effects of shear flow on the kinetics of ordering and/or phase separation by suitably driven Ising lattice gas models. Cirillo *et al.* (2005) studied the kinetics of domain growth in the kinetic Ising model with non-conserved dynamics on the $L \times L$ square lattice with nearest neighbor interaction. Using periodic boundary conditions in the horizontal direction, but free boundary conditions in the vertical one, stochastic shear deformations are realized by randomly choosing (according to some rule) a layer y', with uniform probability $1/L$, and attempting a move in which all layers $y \geq y'$ are shifted to the right by λ lattice spacings with a probability $p < 1$. The product $\lambda \times p$ is then proportional to the shear rate. For small shear rates, one observes almost isotropic domain growth, while for large shear rates a pattern of irregular stripes oriented along the x-axis appears. The typical domain linear dimension in the y-direction varies non-monotonically with the time elapsed following the quench.

In a different physical situation, Smith *et al.* (2008) considered the standard (driven) lattice gas model in a thin film geometry, where a phase-separated state exists with an interface oriented along the xz-plane, parallel to the confining walls of the thin film. They then applied a driving field parallel to the walls; this field either acts locally at the walls in the opposite direction or varies linearly with distance along the strip, thus simulating an interface of a fluid under shear similar to experiment (Derks *et al.*, 2006). Smith *et al.* (2008) found that shear flow reduces the interfacial width by suppressing capillary waves. Of course, none of these kinetic Ising models realizes the hydrodynamic interactions present in real fluids under shear, and hence it is unclear to what extent these models can be compared to experiment. Nonetheless, they should be useful for the testing of basic theories.

Problem 10.1 Consider a 40×40 Ising lattice gas with periodic boundary conditions and a field **E** in the y-direction. Calculate the structure factor $S(1, 0)$ as a function of temperature for $E/k_B = 0$ and 10.0.

10.3 CRYSTAL GROWTH

The growth of crystals from a melt or a vapor has been a topic of extensive study because of the technological implications as well as because of a desire to understand the theoretical nature of the growth phenomenon (e.g. Kashchiev *et al.*, 1997; Gilmer and Broughton, 1983). Microscopic simulations of crystal growth have long been formulated in terms of solid-on-solid Kossel models in which particles are treated as 'building blocks' which may be stacked upon each other. (Although this model neglects the expected deviations from a perfect

lattice structure and the corresponding elastic energies, etc., it does provide the simplest approach to growth with the multiple processes to be outlined below.) Particles may be 'adsorbed' from the vapor or melt with some probability and may diffuse from one surface site to another using a rule which is the equivalent of the spin-exchange mechanism for spin systems. No voids or overhangs are allowed and the resultant growth is 'compact'. Three different processes are allowed: deposition, evaporation, and diffusion, and the goal is to understand what the effect of varying the respective rates for each mechanism is.

Three different kinds of 'bonds' are allowed between nearest neighbors, $-\phi_{ss}$ is the average potential energy of a solid–solid pair, $-\phi_{sf}$ is the average potential energy of a solid–fluid pair, and $-\phi_{ff}$ is the average potential energy of a fluid–fluid pair. Thus, the 'cost' of depositing an adatom on the surface can be calculated by counting the number of bonds of each kind which are created or destroyed and calculating the total energy change. From this approach we can write the effective Hamiltonian for the system as ($\varepsilon = \frac{1}{2}(\phi_{SS} + \phi_{ff}) - \phi_{sf}$)

$$\mathcal{H} = -\frac{\varepsilon}{2}\sum_{\langle i,j\rangle}\sigma_i\sigma_j - H\sum_i \sigma_i + V(\{\sigma_i\}), \tag{10.4}$$

where the occupation variable $\sigma_i = +1$ for an occupied site and $\sigma_i = -1$ for an unoccupied site. $\Delta H = \frac{1}{2}(\mu_{vapor} - \mu_{solid})$. The potential V enforces the solid-on-solid approximation and is infinite for unallowed configurations. In the absence of supersaturation, the rates of deposition and evaporation are the same, but in the case of a chemical potential difference between the solid and liquid states of $\Delta\mu$ the relative rate of deposition is

$$k^+ = v\exp(\Delta\mu/k_B T), \tag{10.5}$$

where the prefactor v gives the 'frequency rate' and that for evaporation becomes

$$k_n^- = v\exp(-n\phi_{SS}/k_B T), \tag{10.6}$$

where the number of bonds which must be broken is n. (Note, the chemical potential required for equilibrium is determined by setting the deposition rates and evaporation rates equal to each other for kink sites.) Diffusion of a particle from a site with energy E_A to a nearest neighbor site with energy E_B is given by

$$k_d = v_d\exp[(E_B - E_A)/k_B T], \tag{10.7}$$

where v_d is the 'frequency rate' for diffusion. As the crystal grows, the surface begins to roughen, but the morphology depends upon the competition between all three processes. Characteristic surfaces after growth has proceeded for a short time for both small super-saturation and large supersaturation are shown in Fig. 10.2.

Spiral crystal growth was studied in a similar fashion (Swendsen *et al.*, 1976) but using a Kossel model which contained a dislocation along one crystal edge.

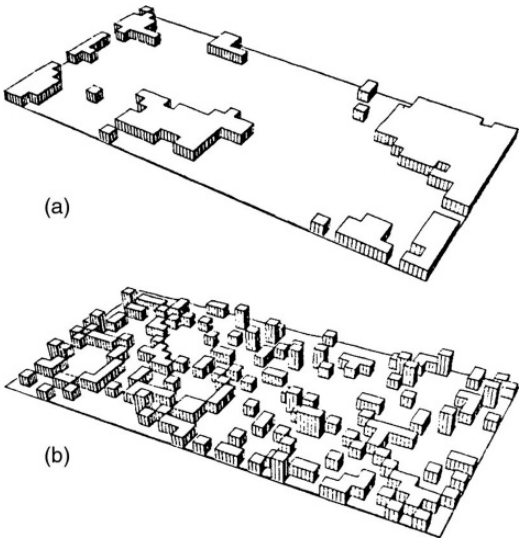

Fig. 10.2 'Snapshots' of crystal surfaces after growth of 25% of a monolayer: (a) $\varepsilon/k_BT = 12$ (ε is the binding energy of a simple cubic crystal) and $\Delta\mu/k_BT = 2$ (only 1.8% of the deposited atoms remained on the surface); (b) $\varepsilon/k_BT = 12$ and $\Delta\mu/k_BT = 20$ (100% of the deposited atoms remained on the surface). From Gilmer *et al.* (1974).

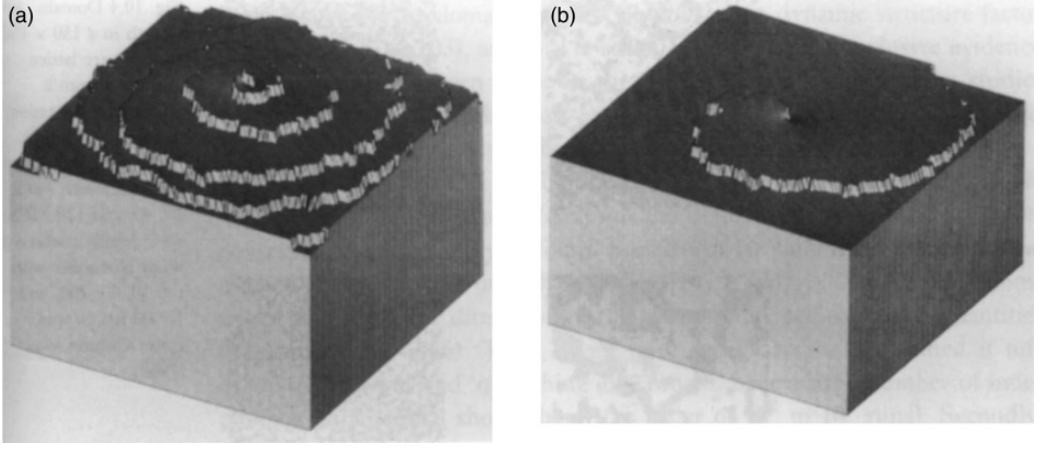

Fig. 10.3 Spiral crystal growth at high temperature for the center 200 × 200 sites of a simple cubic lattice surface: (a) large chemical potential difference $\Delta\mu = 0.6$; (b) small chemical potential difference $\Delta\mu = 0.1$. From Swendsen *et al.* (1976).

Under typical conditions for spiral growth, evaporation is rapid except along the dislocation (growth) edge and heterogeneous nucleation plays essentially no role in the growth. Thus, a standard Monte Carlo simulation of crystal growth used in the first part of this section would lead to extremely slow growth because very few of the deposited atoms would remain on the surface unless they encountered the spiral growth edge. Instead, in the simulation the creation of isolated particles (or holes) in the surface layer was excluded, leading to an increase in the speed of the simulation algorithm by a factor of $\exp(\varepsilon/k_BT)$. This procedure allowed rather large surfaces to be used so that the system could be followed for long enough to permit the formation of multiple spirals. Typical spiral growth is shown in Fig. 10.3. (In some earlier simulations

rather small rectangular systems had been used to simulate the growth along a small strip of the surface which cut through the spirals. In these studies a number of 'steps' were placed on the strip and periodic boundary conditions were applied. The resultant 'growth' resulted in 'step train' behavior, but the spacing between steps was controlled by the number of steps and the lattice size in the direction perpendicular to the steps. Results from the spiral growth algorithm showed that the spacing between spiral arms could become quite large. A 'step train' simulation with multiple steps on a small lattice would thus probably impose an incorrect spacing between the arms and provide results for a system which was inherently non-steady state.)

10.4 DOMAIN GROWTH

The general area of the temporal development of domains spans a wide range of different physical phenomena. Background information about phase separation was provided in Section 2.3 where we saw that at a first order transition regions of aligned spins, i.e. 'domains', would grow as phase separation proceeds. Simple models may be used to study the properties of domains, and the kinetics may be due either to 'spin exchange' or 'spin-flip' mechanisms. The behavior may, in fact, be quite different for different kinetics. For example, in an Ising model which has been quenched to below T_c there will be many small domains formed immediately after the quench, but if spin-flip kinetics are used, some domains will grow at the edges and coalesce but others will shrink and simply disappear, even from their interior. Eventually all 'large' domains except one will disappear with a few overturned spin clusters remaining as a result of thermal excitation. With spin-exchange kinetics the size of the domains is expected to grow with time, but the overall magnetization remains constant; thus two equal size domains will result in the long time limit.

The exponent which describes the domain growth is dependent upon the kinetic mechanism, although a considerable amount of time may need to pass before the asymptotic behavior appears. For non-conserved order parameter models the mean domain radius $\overline{R}$ grows as

$$\overline{R} = Bt^x, \tag{10.8}$$

where $x = \frac{1}{2}$. In contrast for conserved order parameter, the domain growth is much slower and proceeds as given in Eqn. (10.8) but with $x = \frac{1}{3}$. Examples of each kind of domain growth are shown in Fig. 10.4 for the Ising square lattice (after Gunton *et al.*, 1988). While in the Ising model shown in Fig. 10.4 there are just two types of domains (up and down are represented by black and white as usual) and only one kind of domain wall exists, the situation is more subtle when one considers generalizations to more complicated lattice model problems like domain growth in the Potts model (Grest and Srolovitz, 1985), or Ising antiferromagnets with competing nearest and next-nearest neighbor exchange that exhibit a four-fold degenerate groundstate (Sadiq and Binder, 1984), or Ising models with annealed or quenched impurities (Mouritsen,

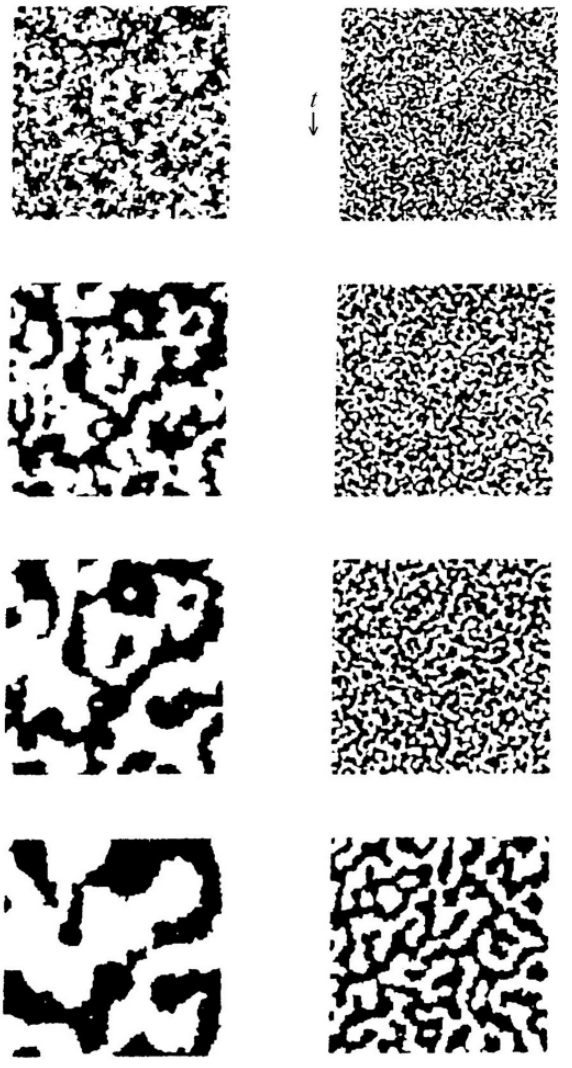

Fig. 10.4 Domain growth in a 150×150 Ising square lattice quenched from a random configuration to $T = 0.6T_c$: (left) non-conserved order parameter with $t = 2$, 15, 40, and 120 MCS/spin; (right) conserved order parameter with $t = 10$, 60, 200, and 10 000 MCS/spin. From Gunton *et al.* (1988).

1990), etc. In many of these models the asymptotic growth laws for the domain radius $\overline{R}(t)$ and for the dynamic structure factor $S(\mathbf{q}, t)$ cf. Eqn. (2.108b), are not yet sorted out with fully conclusive evidence (and the situation is even worse for the analogous molecular dynamics studies of domain growth for realistic off-lattice models of various pure fluids or fluid mixtures, as briefly reviewed by Toxvaerd (1995)).

The reasons for these difficulties come from several sources: first of all, neither the structure factor $S(\mathbf{q}, t)$ nor the domain size – which in the non-conserved case can simply be found from the order parameter square $\psi^2(t)$ at elapsed time t after the quench as $\overline{R}(t) = [\psi^2(t)/\langle\psi\rangle_{eq}^2]^{1/d}\ L$ in d dimensions, where L is the linear dimension of the system – are self-averaging quantities (Milchev *et al.*, 1986). Thus, meaningful results are only obtained if one

averages the simulated 'quenching experiment' over a large number of independent runs (which should be of the order of 10^2 to 10^3 runs). Secondly, often several mechanisms of domain growth compete, such as evaporation and condensation of single atoms on domains may compete with the diffusion and coagulation of whole domains, etc., and thus there are slow transients before one growth mechanism wins. As a consequence, it is necessary to study times where $\overline{R}(t)$ is very much larger than the lattice spacing, but at the same time $\overline{R}(t)$ must be very much smaller than L, because otherwise one runs into finite size effects which invalidate the scaling behavior postulated in Eqn. (2.108). From these remarks it is already clear that the computational demands for obtaining meaningful results are huge. A further difficulty is that random numbers of high quality are needed, since the 'random' fluctuations contained in the initial disordered configuration are dramatically amplified. If there are some hidden long range correlations in this initial state – or if the random numbers used in the growth process would introduce such correlations – the growth behavior could become disturbed in a rather artificial manner. This caveat is not an academic one – in fact in their study of domain growth for the ϕ^4 model on the square lattice Milchev *et al.* (1986) ran into this problem.

Nevertheless, simulations of domain growth and of phase separation kinetics have played a very stimulating role both for the development of analytical concepts on the subject, as well as for experiments. For example, scaling concepts on the subject such as Eqn. (2.108) were postulated some time ago (Binder and Stauffer, 1974) in an attempt to interpret corresponding early simulations. This type of scaling now can be derived from rather elaborate theory (Bray, 1994) and has also been seen in experiments both on phase separation (Komura and Furukawa, 1988) and on the ordering kinetics of monolayers adsorbed on surfaces (Tringides *et al.*, 1987). Thus, the above caveats are by no means intended to prevent the reader working on such problems, but rather to make the pitfalls clear.

Recent work (Mitchell and Landau, 2006) has extended Monte Carlo studies of domain growth to compressible Ising models for which spins are no longer restricted to the sites of a rigid lattice and there is an elastic energy stored in nearest neighbor bonds, i.e. the spins are on a distortable net. This model included a bond angle energy term to ensure stability with respect to shear. Distortable nets as large as 512×512 were used and the 'mismatch', i.e. difference in bond lengths for $++$ and $--$ pairs of spins, was varied. With no mismatch the domain growth was virtually indistinguishable from that for the rigid lattice, but as the mismatch increased a pronounced asymmetry in different directions was visible.

The results for the time dependence of the domain size, shown in Fig. 10.5, strongly suggest that the dynamic growth exponent 'x' (see Eqn. (10.8)) changes with mismatch. This intriguing result further raises the question about the nature of any possible dynamic universality. Much remains to be done before we can claim a broad understanding of (non-equilibrium) domain growth. For theoretical background on this problem, see Onuki (2002).

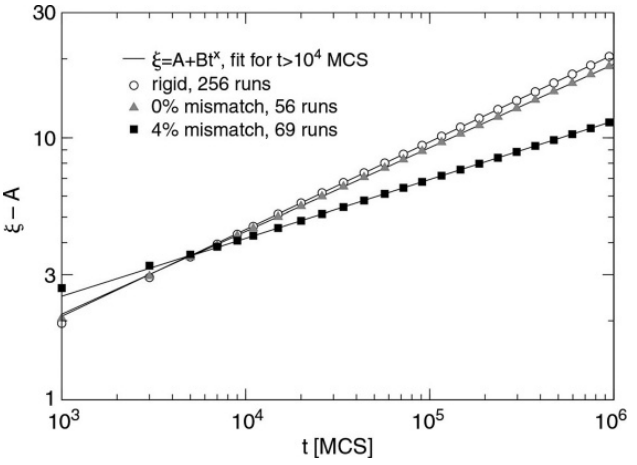

Fig. 10.5 Time dependence of the domain size $\zeta(t)$ in a compressible Ising model; $L = 512$ and data are averaged over multiple runs and directions. Solid lines are from non-linear fits to $\zeta(t) = A + Bt^x$, where x is the domain growth exponent and A is the first 'correction' term. Error bars are much smaller than the symbol size. After Mitchell and Landau (2006).

Problem 10.2 Consider a 40×40 Ising model with periodic boundary conditions. Starting with a random spin configuration, use Kawasaki dynamics to carry out a Monte Carlo simulation at $T = 1.5\ J/k_B$. Measure the mean domain size.

10.5 POLYMER GROWTH

10.5.1 Linear polymers

The study of the growth of linear polymers from a solution may be easily modeled using very simple models. We begin with a lattice filled with bi-functional monomers, i.e. each monomer may form only two bonds. Each monomer is allowed to randomly atttempt to form bonds with nearest neighbors subject, of course, to the limitation in the number of bonds per monomer. A series of linear polymers will result. If bonds are also allowed to break, the model is appropriate for reversible polymerization, otherwise the polymerization is irreversible. If empty sites are included, they may play the role of solvent atoms. As a result of the growth process a distribution of chain lengths and radii of gyration will result.

10.5.2 Gelation

The formation of cross-linked polymers, such as gels, is an extremely important problem which is of particular interest for those who are developing new 'designer materials'. The study of addition polymerization and the subsequent formation of gels is a problem which is well suited for simulation (Family and

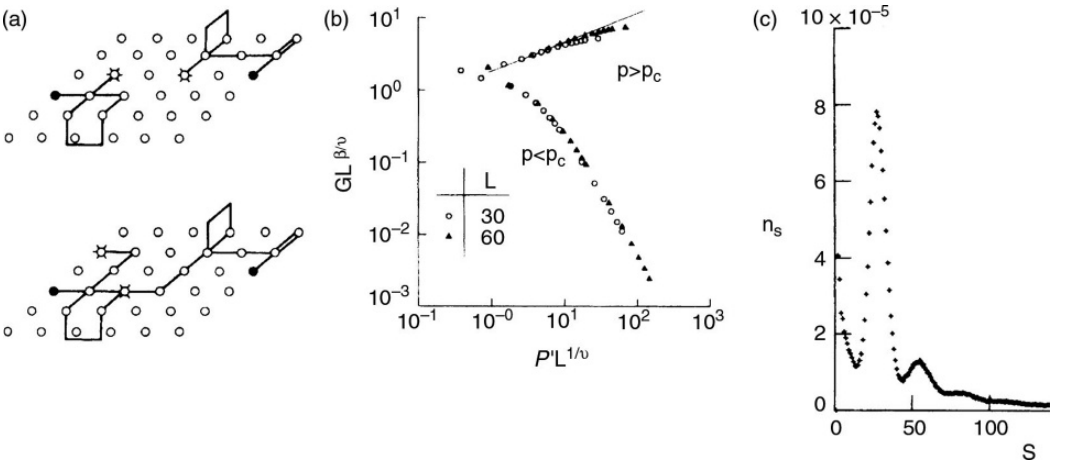

Fig. 10.6 Kinetic gelation model: (a) schematic view of growth within a single layer of a three-dimensional model just before and just after two growing clusters link up, the solid dots show the initial positions of the initiators and data for the cluster size distribution; (b) finite size scaling plot for the gel fraction for $c_I = 3 \times 10^{-2}$; (c) cluster size distribution for $c_I = 3 \times 10^{-4}$ and $p = 0.16$. From Chhabra *et al.* (1986).

Landau, 1984). We describe the kinetic gelation model for irreversible, addition polymerization, see Manneville and de Seze (1981) and Herrmann *et al.* (1983), in which we begin with a lattice which contains a mixture of bi-functional and four-functional monomers. In addition, there are a few randomly placed radicals (with concentration c_I) which serve as initiators for the growth process. When a bond is formed between a monomer and an active site (initially an initiator site), the unpaired electron is transferred to the newly bonded site and it becomes 'active'. In addition polymerization, growth may only proceed from these active sites. Bi-functional monomers can only participate in a self-avoiding walk process, whereas the four-functional monomers may be involved in loop formation and cross-linking between growing chains. Initially the solution of unconnected monomers is called a 'sol', but as the growing chains link up they may form an infinite cluster called a gel. This process may involve a phase transition known as the sol–gel transition in which a finite fraction of the system is in the largest cluster. This is analogous to the percolation transition discussed in Chapter 4. Figure 10.6a shows a schematic view of a portion of a three-dimensional system in which gelation is occurring (see Chhabra *et al.* (1986)). The gel fraction G plays the role of the size of the largest cluster in percolation, and its behavior can be analyzed using finite size scaling (see Fig. 10.6b) just as in the case of percolation. Unlike percolation, however, the cluster size distribution n_s is *not* monotonically decreasing. As shown in Fig. 10.6c there are distinct peaks in the distribution at characteristic values of s. These peaks result from the approximately uniform growth of each cluster until two clusters of size s_o combine to form a single cluster of size $2s_o + 1$. Since the characteristic size of the smallest 'unit' of the system as it approaches the sol–gel transition becomes a cluster, rather than a monomer, very large lattices are needed for the simulations.

10.6 GROWTH OF STRUCTURES AND PATTERNS

The formation of structures due to diverse growth mechanisms offers a rich and rapidly growing area of investigation (Herrmann, 1986a) which we can only briefly treat here.

10.6.1 Eden model of cluster growth

First designed as a simple model for cancer growth, the Eden model (Eden, 1961) allows the study of growing compact clusters. Growth begins with a seed particle, one neighboring site of which is then randomly occupied. Then, one neighboring site of the enlarged cluster is occupied, and the process continues in the same fashion. Perhaps the most interesting question about the growth process is the nature of the surface after growth has proceeded for a long time, i.e. how does the width of the surface depend upon the total number of particles which have been added?

In the actual implementation, one may construct a list of the 'growth sites', i.e. a list of perimeter sites which are adjacent to the cluster and at which new particles may be added. A separate array is used to keep track of those sites which have never been touched. At each step of the growth process a site is randomly chosen from the perimeter list. (The alternative approach, of searching for nearest neighbors of 'surface sites' has the danger that some sites may be chosen with too high a probability, i.e. a site may be the nearest neighbor of two different surface sites.) This site is removed from the perimeter list and one must then check to see if any of its neighboring sites have not been touched. If so, they are added to the perimeter list before the next particle is added.

10.6.2 Diffusion limited aggregation

Diffusion limited aggregation (DLA) was first proposed as a simple model for the description of the formation of soot (Witten and Sander, 1981). It has played an extraordinary role, not only in the development of the examination of fractal matter, but also in the use of color coding to effectively portray a third dimension, time, in the development of the system. The fundamental idea of DLA growth is quite simple. A 'seed' particle is placed in the center of the system and another particle is turned loose from a randomly chosen point on a large 'launch circle' which surrounds the seed. This new particle executes a random walk until it encounters the seed particle and then sticks to it. At this point another particle is turned loose from the launch circle and the process is repeated. A beautiful, fractal object results from this procedure and we find that the outer arms of the growth object shield the inner 'fjords' from the particles which are released at later times. Particles may be color coded according to the time at which they were released, and the distribution of adsorbed particles of different colors provides information about the effective

'shielding' of different portions of the cluster. The fractal dimension d_f of the DLA cluster can be determined by measuring the mass M of the cluster within a radius R of the seed and using the relation

$$M \propto R^{d_f} \tag{10.9}$$

to extract an estimate. The effective fractal dimension as a function of cluster size and dimension has been the object of extensive study (Barabási and Stanley, 1995); in two dimensions, DLA clusters with more than 10^7 particles have been grown and the fractal dimension has been estimated at $d_f = 1.71 \pm 0.01$. It was realized fairly quickly that for large systems on a lattice, effects of the anisotropy imposed by the lattice structure began to affect the properties of the cluster. Thus, DLA clusters have been grown in continuous space ('off-lattice') as well as on a variety of lattices.

10.6.2.1 On-lattice DLA

As is often the case, the restriction of a model to a lattice simplifies the situation and enables the use of time saving tricks. In the most straightforward implementation of the DLA algorithm, the particles execute a simple random walk on the lattice with each step being of unit length in a random direction. Each particle is started from a random position on a circle which has the seed at its center. (As the DLA cluster grows, the radius of this 'launch circle' is increased so that it remains larger than the greatest extent of the cluster.) The random walk process is very slow in reaching the growing cluster and can be accelerated in a very simple fashion. The lattice sites surrounding the growing cluster are each assigned an integer which is large far away from the cluster and becomes smaller as the distance to the cluster decreases. This integer specifies the size of the random step that the particle will take when it moves from that site. In the immediate vicinity of the growing DLA cluster the movement reverts to a simple nearest neighbor random walk. An example of the structure which results from this procedure is shown in Fig. 10.7a. For comparison, in Fig. 10.7b we show a pattern which was produced in a Hele–Shaw cell by pumping air into liquid epoxy which filled the spaces between a monolayer of glass balls, all between two parallel glass plates. As the size of the cluster increases, the shape of the cluster begins to reflect the underlying lattice. This effect can be made even more pronounced by using the technique of 'noise smoothing': a particle is finally absorbed only after it has experienced N-collisions, where the integer N becomes a parameter of the simulation and may be varied. The result is a structure which is much more anisotropic than for a simple DLA.

10.6.2.2 Off-lattice DLA

Growth on a lattice is intrinsically affected by the presence of the underlying lattice structure. Any such effects can be removed simply by avoiding the use of a lattice. Eliminating the use of a lattice complicates the simulation and, in

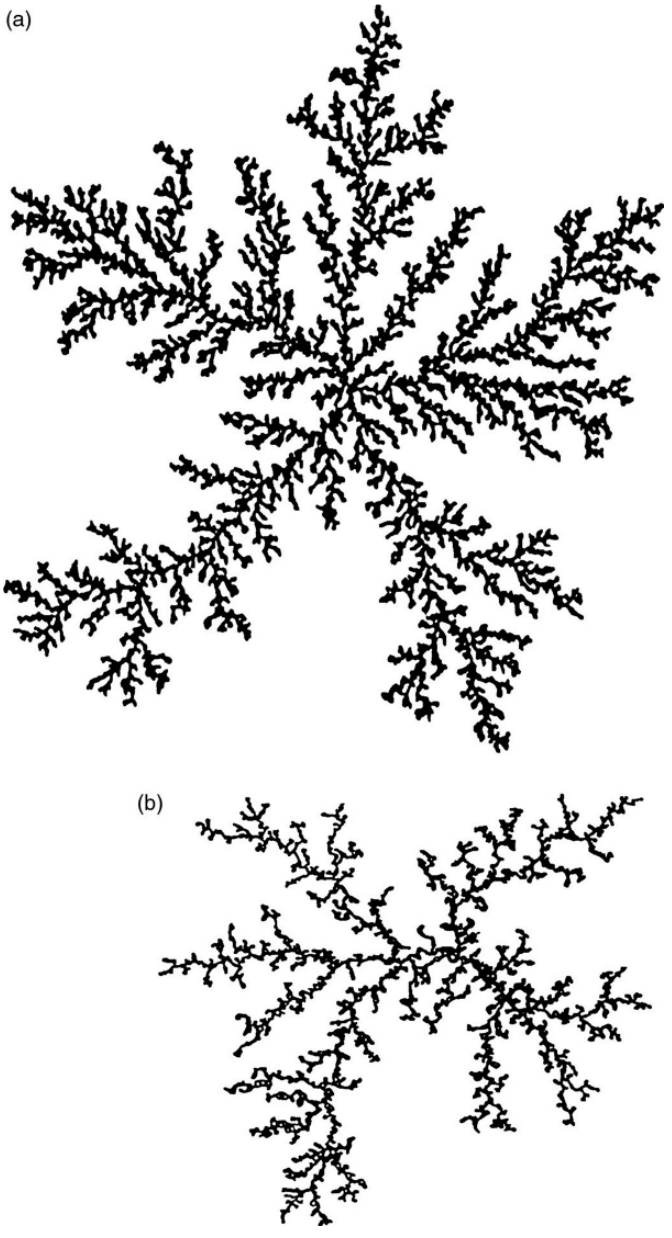

Fig. 10.7 (a) DLA cluster of 50 000 atoms grown on a square lattice (Feder, 1988); (b) Hele–Shaw cell pattern resulting from air displacing liquid epoxy in a monolayer of glass spheres (Måløy *et al.*, 1985).

particular, the determination of when a particle actually encounters the cluster becomes non-trivial, but it does also remove any effects attributable to any underlying anisotropy. It becomes necessary to compute a trajectory for each step of the random walk and check to see if the particle touches the cluster at some point along its path. If so, the particle is attached to the cluster at that point and a new particle is released from the launch circle so that the growth process proceeds just as for the on-lattice case.

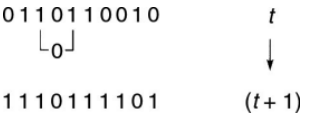

Fig. 10.8. Example of the time development of a simple cellular automaton using a nearest neighbor XOR rule.

Problem 10.3 Grow a DLA cluster on a square lattice with 10 000 particles. Then grow a DLA cluster of the same size on a triangular lattice. Comment on the similarities and the differences between the two clusters.

10.6.3 Cluster–cluster aggregation

An alternative growth mechanism involves the simultaneous activity of many 'seeds' through the consideration of an initial state which consists of many small clusters (Jullien *et al.*, 1984). Each cluster is allowed to diffuse randomly, but if two clusters touch at any point, they stick and begin to move as a single cluster. This model is expected to be well suited to the study of colloid formation and the coagulation processes in, for example, aerosols. In the simplest case, the clusters all move at the same speed. A more realistic approach is to allow the speed of a cluster to depend upon the inverse of the mass of the cluster, i.e. $\sim m^{\alpha}$. The choice of the exponent α does not affect the fractal dimension of the resulting aggregates except at very low concentrations but it does enter the distribution function and the dynamical behavior.

10.6.4 Cellular automata

Cellular automata are simple lattice or 'cell' models with deterministic time dependence. The time development can, however, be applied to many of the same systems as Monte Carlo processes, and methods of analysis of cellular automata have impacted stochastic simulations. For completeness, we shall thus say a few words about cellular automata. A more complete treatment of this topic is available in Herrmann (1992). These models are defined by a collection of 'spins' or 'cells' on a d-dimensional lattice where each cell contains either a '0' or a '1'. Time is discretized and the value of a cell, σ_i, at time $(t+1)$ is determined by a simple 'rule' which involves the local environment of the ith cell at time t. A simple example is the XOR (exclusive-or) rule in which $\sigma_i(t+1) = \sigma_{i-1}(t)$ .XOR.$\sigma_{i+1}(t)$. Different rules result in quite different dynamic features; some produce patterns which are simple and others produce quite complex structures in time. An example of the 'growth' of a one-dimensional cellular automaton, i.e. the time development, with an XOR-rule is shown in Fig. 10.8. The application of the rule to a single site is shown along with the full configurations at times t and $(t+1)$. The major question to be answered is 'what is the nature of the behavior after a long time has elapsed?' One very simple approach is to study the 'damage spreading' (Stauffer, 1987). Consider two cellular automata which follow the same rule.

Choose initial states which are identical except for some small region which is different, i.e. 'damaged' in one system. Allow both systems to propagate forward in time and then see what happens to the damage. The damage may disappear completely with the passage of time, may remain localized, or may spread throughout the system. This latter behavior is indicative of the onset of chaos as is only observed for a small fraction of the rules. An equivalent approach can be taken in Monte Carlo simulations by considering two systems with almost identical initial states. The same random number sequence is then used in a simulation of each system, and the differences in the configurations for the two systems are then followed as a function of time. The critical dynamics of a cellular automata rule called Q2R in two dimensions appears to be consistent with model A Ising behavior (or possibly model C), but in three dimensions the behavior appears to be quite different (Stauffer, 1997).

Using a random initial configuration, one can model the Ising model by a Q2R cellular automaton in which a spin is flipped only if it involves no change in energy (Herrmann, 1986b). This can be carried out quite efficiently if the checkerboard decomposition is used. Unfortunately the cellular automaton algorithm is not ergodic. A solution to this problem is to randomly flip a spin occasionally while maintaining the energy within a narrow band of energies.

Probabilistic rules, e.g. the Hamiltonian formulation of the Kauffman model, may also be used.

Problem 10.4 Use the nearest neighbor XOR rule described in Fig. 10.8 to follow a 32-bit cellular automaton with p.b.c. in time with the following initial conditions: (a) a single bit is 1 and all other bits are 0; (b) 16 of the bits (randomly chosen) are 1 and the other bits are 0.

10.7 MODELS FOR FILM GROWTH

10.7.1 Background

The growth of films and the characterization of the resultant surface has formed a topic of great experimental, theoretical, and simulational interest. One standard measure of the nature of this growth surface, whose local position at time t is $h(\mathbf{r}, t)$, is given by the long-time dependence of the interfacial or surface width W,

$$W^2(t) = \langle h^2 \rangle - \langle h \rangle^2, \tag{10.10}$$

which diverges as $t \to \infty$. Note that the mean position of the surface $\langle h \rangle$ is given merely by the rate at which particles are deposited and is uninteresting. The manner in which the surface width diverges can be described by a 'critical' or growth exponent which places the systems into 'universality classes' which are analogous to the classes that have been identified for static critical behavior.

Thus, the temporal variation of the surface width after growth has proceeded for a long time may be given by

$$W(t \to \infty) = Bt^{\beta}, \tag{10.11}$$

where the prefactor B is relatively unimportant but the growth exponent β defines the nature of the growth. In a finite system the surface width saturates at long times and instead it is the size dependence of the saturated width which is of interest:

$$W(L \to \infty) = AL^{\alpha} \tag{10.12}$$

where α is termed the 'roughening' exponent. The ratio of the exponents defines a dynamic exponent z, i.e.

$$z = \alpha/\beta. \tag{10.13}$$

The time-dependent and size-dependent behavior can be condensed into a dynamic scaling relation (Vicsek and Family, 1985)

$$W = L^{\alpha}\mathcal{F}(tL^{-z}) \tag{10.14}$$

which should be valid in a general case. Since both relations, Eqns. (10.11) and (10.12), hold only in the asymptotic limit of large substrate size and long times, the extraction of accurate estimates for these exponents is non-trivial. These relations are expected to be generally valid, so we may attempt to analyze the behavior of many growth models using this formalism.

10.7.2 Ballistic deposition

Growth models such as ballistic deposition (see Barabási and Stanley, 1995) are relatively easy to study and the results can be displayed and interpreted graphically. In the simplest case particles are dropped from random positions above a surface and fall in a straight line until they either land on the surface or encounter a particle which has already been deposited. In the latter case, the new particle sticks to the old one either on the top or on the side. Particles are dropped sequentially and a very perforated structure grows. From a computational perspective ballistic deposition is very easy to simulate. For deposition onto a line, we randomly choose a horizontal position x_n and check to find the height of the uppermost occupied site y_n in the column above x_n and that of its two neighbor columns, i.e. y_{n-1}, y_{n+1}. If y_n is the largest of these numbers, the particle is deposited at height $(y_n + 1)$; if one of the neighboring columns is higher, the particle is deposited at a height which is the highest of $(y_{n-1} + 1)$ or $(y_{n+1} + 1)$. For deposition using a point seed, the process proceeds exactly the same as for the line 'substrate', but most of the particles never strike the seed, at least at early times. As an example, in Fig. 10.9 we show a ballistic deposition cluster which has resulted from growth with a point seed.

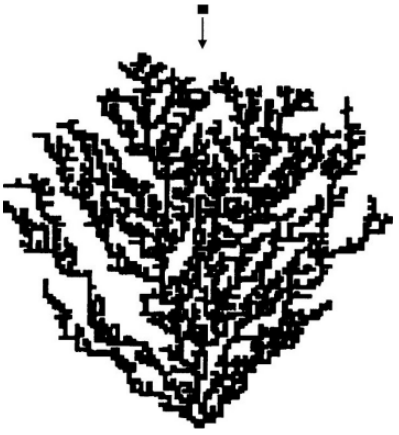

Fig. 10.9 Pattern formed by ballistic deposition simulation using a point substrate.

10.7.3 Sedimentation

In an effort to describe growing surfaces which are more compact than those described by ballistic deposition, Edwards and Wilkinson (1982) introduced a simple model which could be solved exactly. In this EW model, a particle is dropped from a random position above a growing surface. The particle lands on top of the column below the point from which it is dropped and then diffuses once to the neighboring site which is lowest lying. Another particle is then dropped and the process is repeated. Edwards and Wilkinson (1982) map this model onto a simple differential growth equation in which the variable h_i is the height of the growing surface above the mean position and

$$\frac{\partial h}{\partial t} = v\nabla^2 h + \zeta(r, t), \tag{10.15}$$

where v is the surface tension and $\zeta\ (r, t)$ is δ-correlated noise in both space and time. The solution to this differential equation yields a dynamic exponent $z = 2.0$. However, in the simulation of the atomistic model an interesting question arises: what does one do when there is more than one neighboring site of the same 'lowest' depth? While it might seem intuitive to make a choice between the different possibilities by generating a random number, this procedure in fact leads to an additional source of (correlated) noise and changes the value of z. If a particle with multiple choices does not diffuse at all, diffusion becomes deterministic and $z = 2$ is recovered. This finding points out the subtleties involved in obtaining a complete understanding of film growth (Landau and Pal, 1996; Pal and Landau, 1999; Pal *et al.*, 2003).

There are variations of this model, e.g. by Wolf and Villain (1990), which use different rules for hopping and which result in different behavior. (For example, in the WV model, particles hop to the nearest neighbor site in which they will have the greatest number of bonds rather than the lowest height.) All of these models may be compared with the KPZ model (Kardar *et al.*, 1986), which is defined by a differential equation that includes the tilt of the surface and the surface curvature. One issue that remains to be resolved is

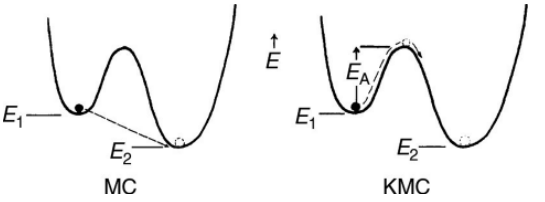

Fig. 10.10 Schematic comparison between Monte Carlo and kinetic Monte Carlo methods for diffusion of surface adatoms between two sites with energy E_1 and E_2, respectively. E_A is the activation energy for KMC.

the delineation of the criteria which determine non-equilibrium universality classes.

Problem 10.5 Grow a (1 + 1)-dimensional Edwards–Wilkinson film for substrate lattices of size $L = 20$, 40, and 80. Measure the interfacial widths and plot them as a function of time. Estimate α, β, and z.

10.7.4 Kinetic Monte Carlo and MBE growth

More recently, attention has turned to the simulation of thin films grown by molecular beam epitaxy (MBE). The growth of films by MBE requires the inclusion of both deposition and diffusion processes. Some efforts have been directed at fully understanding the behavior of relatively realistic models for small films using empirical potentials for short times, and other studies have been directed at the scaling behavior of simpler models. In this section we shall concentrate on the simplest, lattice models for MBE growth. This approach is also in terms of solid-on-solid models with nearest neighbor interactions. Particles are deposited with some fixed flux **F**. Any of the particles may then undergo activated diffusion with probability

$$p = \exp(-E_A/kT). \tag{10.16}$$

For simple models with nearest neighbor coupling, the activation energy may be simply dependent upon the number of occupied nearest neighbors, i.e. $E_A = \mathcal{J} \sum n_j$. An atom which has been activated may then hop to a nearest neighbor site either randomly or with a probability which depends upon the energy that the atom will have in that site. Thus, the rate of hopping does not depend merely upon the relative energies of the configuration before and after hopping as it would in a simple 'spin-exchange' Monte Carlo process but rather the barrier plays an essential role. Diffusion thus proceeds via a two-step process and the simulation technique which matches this process is called kinetic Monte Carlo. Kinetic Monte Carlo methods also find widespread application for the study of surface diffusion in adsorbed monolayers (see e.g. Uebing and Gomer, 1991, 1994). This application is also discussed at the end of Section 4.4.3 on diffusion and in the references quoted there. The differences between the two processes are shown schematically in Fig. 10.10.

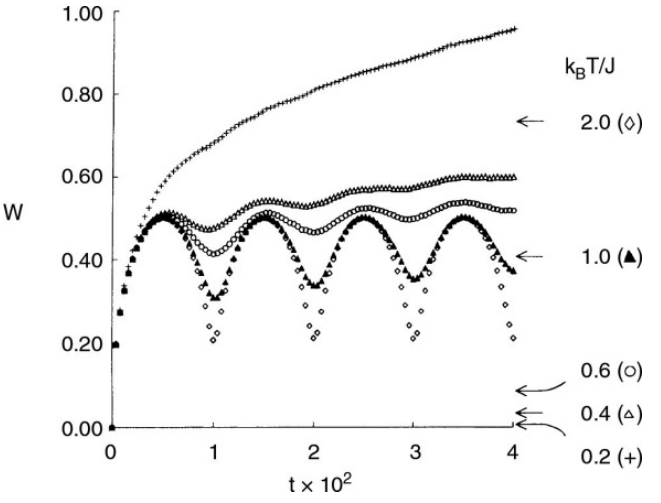

Fig. 10.11 Time dependence of the surface width for MBE models on $L \times L$ substrates with p.b.c. Values of the surface width for equilibrium are shown by the arrows to the right. After Pal and Landau (1994).

The nature of the growth depends upon the magnitude of the flux as well as the temperature. At very low temperatures there is little diffusion and the surface width grows monotonically as shown in Fig. 10.11. As the temperature is raised oscillations in the data indicate layer-by-layer like growth, i.e. atoms which land on a 'plateau' diffuse off the edge and nucleation of a new layer begins only after the layer below is filled. (Calculations of the RHEED intensity from the surface configuration generated show that even at the very lowest temperature studied there are small oscillations remaining, and at sufficiently long times the width diverges for the higher temperatures shown in Fig. 10.11 for preferential hopping. Thus, there is no true transition between layer-by-layer growth and rough growth.) Note that Fig. 10.11 compares the equilibrium surface width with that obtained for the MBE growth model: the trends for the variation of the mean surface width are exactly reversed because the equilibrium surface width is quite small at low temperatures. The growth process may be repeated multiple times with different random number sequences. Each of the resultant 'growth histories' is independent, so that statistical accuracy can be improved by simply taking the average over many runs and the error bars are then straightforward to calculate. Of course, data for successive times for a given simulation will be correlated, so care must be exercised in analyzing 'structure' which is seen in a single run or a small number of runs. The long time behavior can be difficult to ascertain, because the 'asymptotic region' appears for quite different times for different values of the relevant parameters. Extensive simulations have shown that it is possible to find quite different 'effective' growth exponents for different fluxes, and we recommend that a particular exponent be observed to describe the data over *at least* two decades in time before being deemed acceptable. Finite size effects also become important at long time and dynamic finite size scaling, Eqn. (10.14), can be used to analyze the data and extract exponent estimates. A typical finite size scaling plot for the surface width of a $(2 + 1)$-dimensional

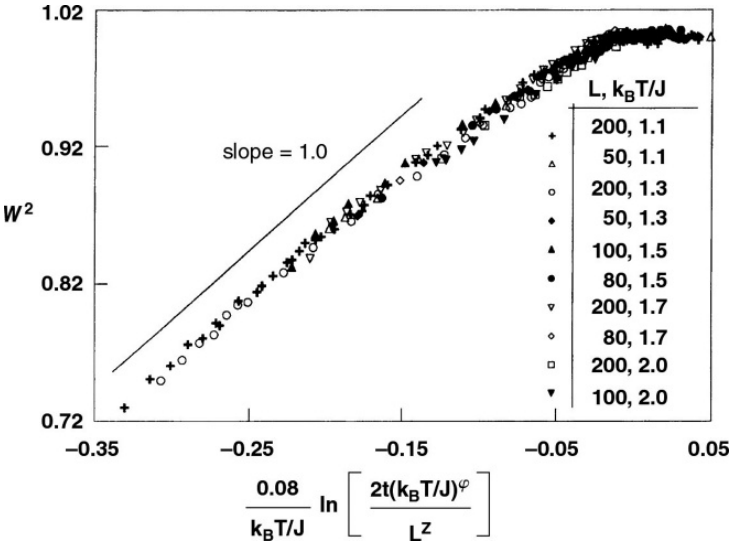

Fig. 10.12 Dynamic finite size scaling of the surface width for $(2+1)$-dimensional MBE models. The growth exponent $\beta = 0$, $\phi = 3.85$ and the dynamic exponent $z = 1.63$ for this plot. From Landau and Pal (1996).

MBE growth model is shown in Fig. 10.12. Note that scaling of the surface width can be made to include the temperature dependence.

Problem 10.6 Grow a (1 + 1)-dimensional MBE film using a KMC method with a deposition rate of 1 layer/sec and a prefactor for activation of 0.1. Plot the interfacial width, averaged over multiple runs, as a function of time for $L =$ 20, 40, and 80. How does the time at which finite size effects become obvious vary with L?

Problem 10.7 Grow a (1 + 1)-dimensional MBE film using 'spin exchange' Monte Carlo with a deposition rate of 1 layer/sec and a diffusion rate constant of 0.1. Plot the interfacial width as a function of time for $L = 20$. Compare your result with that obtained by kinetic Monte Carlo in Problem 10.6.

10.8 TRANSITION PATH SAMPLING

While standard Metropolis-type importance sampling Monte Carlo is designed to generate statistical information about a state point of a statistical mechanical system, a different problem not addressed by this algorithm is the nature of a transition path from one state, A, of the system to another state, B. Such a transition may be a phase transition caused by a sudden change of external variables such that the state A is now only metastable while the state B is the stable one. A generic example for this problem is the Ising (or lattice gas) model, where we begin with a positive magnetization but at time $t = 0$ apply a weak negative magnetic field to the system. Roughly speaking one knows that the kinetic pathway by which the new phase (with negative magnetization) appears involves nucleation and growth. Within the framework of a kinetic Ising model description, the task is to generate a statistical sample of the transition paths by which the system may develop. Of course, the nucleation of critical clusters,

corresponding to a saddle point configuration in the (free) energy landscape of the model, is a rare event; and hence a naïve sampling (along the lines of simulations of critical relaxation of kinetic Ising models as described in Section 4.2.5) of these kinetic pathways would be impractical.

The problem mentioned above is addressed by 'transition path sampling' (Dellago *et al.*, 2001; Bolhuis *et al.*, 2002) which avoids spending a large part of the total simulation effort on simulating the initial metastable state (as the naïve straightforward simulation approach to the problem would do), but instead attempts to sample almost exclusively the 'reactive parts' of the trajectories. Although the notion of a 'reaction coordinate' (e.g. the size of the nucleated cluster or nucleation event) is implicit, no reaction coordinate is required *a priori*. The idea is to use one trajectory which leads from A to B as an initial trajectory to generate new trajectories in much the same spirit as in the standard Metropolis method where one state point is used to construct a new state point by a suitable transition probability. In this way one can find a 'transition state ensemble': e.g. in nucleation it is not a simple cluster configuration which defines the transition state but an entire ensemble of cluster configurations (because the 'critical nuclei' are randomly fluctuating in their shape). Thus, two 'cluster coordinates', such as volume and surface area of the cluster, may not be adequate, as pointed out already by Binder and Stauffer (1976). Transition path sampling provides an elegant framework to address not only this problem but a whole class of related problems. A sound theoretical basis for this approach has recently been developed by Van den Eijnden (2006), i.e. the so-called 'transition path theory'. Since the implementation of this new method is still under development, and is somewhat technical, we refer the interested reader to the quoted literature for details.

10.9 FORCED POLYMER PORE TRANSLOCATION: A CASE STUDY

Translocation of a polymer through a narrow pore in a membrane is a non-equilibrium process that is important for many problems in biology, e.g. injection of viral DNA into a host cell, packing of DNA into a shell in the course of viral replication, gene swapping through bacterial pili, etc. (Alberts, 1994). This process is also of interest for practical applications, such as gene therapy (Hanss *et al.*, 1998), cell transformation by DNA electroporation (Alberts, 1994), etc. Experiments, where DNA migrates through microfabricated channels (Han *et al.*, 1999) or through protein channels in a membrane (Meller *et al.*, 2001), are further motivated by the possibility to determine a DNA or RNA sequence by tracking its passage through a pore (Meller *et al.*, 2001; Meller, 2003).

Despite the complexity of the chemical and geometrical structure of biopolymers and biological membranes, theoretical ideas on the subject have largely ignored this complexity, considering as a model a flexible homopolymer threading through a hole in (an infinitely thin) and otherwise impenetrable

plane (Park and Sung, 1998; Muthukumar, 1999). The polymer is pulled through either by a difference in chemical potential acting on the monomers on opposite sides of the wall, or by an adsorption energy acting on one side of the wall (Park and Sung, 1998; Milchev *et al.*, 2004), or by pulling the chain at one chain end (Kantor and Kardar, 2004) (which can be done by attaching a latex ball to a chain end and manipulating the latex ball with an optical tweezer (Farkas *et al.*, 2003)). Note that the chemical potential difference across a membrane is produced (for monomers carrying an electric charge) via an electrical voltage $2V$ between the two sides of the membrane, which in a Monte Carlo context (Vocks *et al.*, 2008) means that for monomers entering the hole in the membrane and passing through it from left to right, an energy $2qV$ is won. Similarly, a force on the chain end can be realized by a bias in the hopping rate in the $+x$-direction, i.e. from left to right (Kantor and Kardar, 2004; Dubbeldam *et al.*, 2007). In the limit of infinite force, jumps of the end monomer in the $-x$-direction are completely forbidden. The polymer configurations look very different for different translocation conditions, and in Fig. 10.13 we show snapshots of polymers being pulled through a pore by applying an infinite force to one end or by the imposition of an infinite chemical potential difference between the two sides (Kantor and Kardar, 2004).

While analytical models have described the process as a diffusion (Sung and Park, 1996; Muthukumar, 1999) or fractional diffusion (Dubbeldam *et al.*, 2007) of a single 'reaction coordinate' $s(t)$ (the monomers are labeled from $s = 1$ to $s = N$ along the chain, so $s(t)$ labels the monomer which is at the pore at time t) over a potential barrier, NEMC simulations in the papers mentioned above have shown that the actual behavior is much more complicated. A general conclusion is that the assumption of the phenomenological theories, that the parts of the chain on the right and left side of the membrane are in local equilibrium, fail. Thus, the monomers execute anomalous diffusion (i.e. with mean square displacement $\langle [r_i(t') - r_i(t)]^2 \rangle \propto (t' - t)^\alpha$ with an exponent $\alpha < 1$), but the value of the exponent differs from that encountered for a Rouse model of a chain that is in equilibrium. In the latter case, $\alpha = 2/(1 + 2\nu)$, where ν is the exponent in the Flory relation for the polymer radius $R \propto N^\nu$ (Kremer and Binder, 1984). How this exponent depends on the type of force pulling the chain through the membrane pore is not well understood. Similarly, the time it takes to pull the chain through the membrane pore is expected to exhibit a power law, $T \propto N^\beta$, but the value of the exponent β is controversial (Vocks *et al.*, 2008). One important complication could be 'memory effects'; i.e. monomers that have just passed through the pore are driven back due to density imbalance. Vocks *et al.* (2008) have probed these memory effects over many decades, and in Fig. 10.14 we show their results for different values of the applied electric field E.

The extent to which a quasi-stationary state is established for times $t = \tau$ is also unclear (Vocks *et al.*, 2008). Note that the process starts from an equilibrated chain conformation where all monomers are to the left of the membrane and only the first monomer is in the pore. At time $t = 0$, the translocation dynamics starts, and then there is a transient period where more

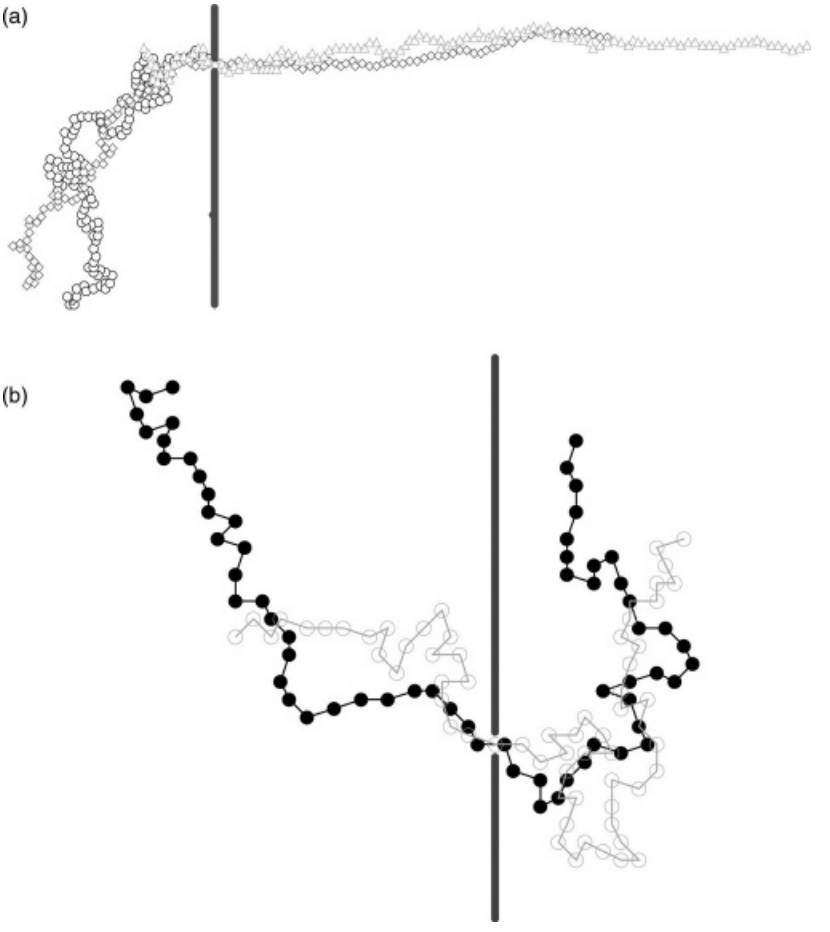

Fig. 10.13 Configurations of a polymer of length N crossing a membrane: (a) $N = 128$, pulled by an infinite force applied to the end. Circles, diamonds, and triangles represent configurations at time $t = 0$, 60 000, and 120 000 MCS; (b) $N = 64$, under an infinite chemical potential difference. Full and open circles represent $t = 10\,000$ and 25 000 MCS. From Kantor and Kardar (2004).

and more monomers pass through the pore, and the left part of the chain, which initially was in equilibrium, is then out of equilibrium. From a theoretical point of view, little is known about such non-stationary, non-equilibrium processes. Kinetic Monte Carlo methods (which for the present models would just reduce to the Rouse model of polymer dynamics, if the chain configuration is in equilibrium) are a very simple and suitable tool to study such processes. (Note that chain lengths of interest are rather long; e.g., Vocks *et al.* (2008) used a lattice polymer with chain lengths $N \leq 1200$ and averaged over many thousands of translocation events to obtain meaningful statistics. Mean square displacements and other dynamic characteristics were then followed over many decades.)

Polymer translocation is an example, where referring back to the triangle in Fig. 1.1, the simulational approach still is hampered by insufficient input from analytical theory to guide the analysis of the data. Despite many attempts, many conflicting results have prevented the development of a clear picture, and the controversies about which asymptotic exponents control the behavior

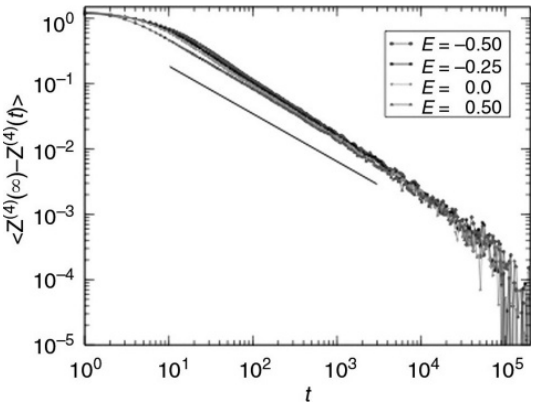

Fig. 10.14 Time dependence of the memory kernels for different electric field strengths E for polymers of length $N = 400$. From Vocks *et al.* (2008).

are referred to as the 'exponent war' in the literature (Panja *et al.*, 2013). Experiment is not yet of great help either, since hydrodynamic interactions between monomers transmitted by the solvent fluid are always present in experimental systems, and trying to incorporate them (e.g. in an all atom Molecular Dynamics study including the solvent molecules explicitly) is even more difficult than a NEMC study. But there is hope that the NEMC studies that already exist (for a review, see Panja *et al.* (2013)) will turn out to be valuable for testing (present and future) theories on this exciting subject.

10.10 THE JARZYNSKI NON-EQUILIBRIUM WORK THEOREM AND ITS APPLICATION TO OBTAIN FREE ENERGY DIFFERENCES FROM TRAJECTORIES

In this section we consider processes where, by changing an external parameter $\lambda(t)$ with time t, we change the Hamiltonian $\mathcal{H}_\lambda(\vec{X})$ of a system continuously from some initial value $\lambda_i(t_i)$ to some final value $\lambda_f(t_f)$. A typical example, motivated by corresponding experimental studies, is the stretching of macromolecules by pulling at their ends. In practice this can be done by chemically attaching suitable colloidal particles at the chain ends of the macromolecule (for simplicity we assume a simple linear chemical architecture). With laser tweezers the distance $X(t)$ between the chain ends can be controlled, and by increasing $X(t)$ from a small value (typical for the coil conformation of a flexible macromolecule) one does work against the elastic restoring forces when the chain is stretched out. Measuring such non-equilibrium force versus extension relations is a broadly used method to study proteins, DNA, and other biopolymers. But for many other soft matter systems a study of the work performed through mechanical deformation processes is also of interest.

From the second law of thermodynamics it is well known that the work W done in such a non-equilibrium state (with free energy F_i) to a final state

(where one again lets the system reach equilibrium, with free energy F_f) cannot be less than the free energy difference,

$$W \geq \delta F = F_f - F_i. \tag{10.17}$$

The equality only holds if the path between the states of the system is reversible, i.e. one is in equilibrium at each of the intermediate states (characterized by $\lambda(t)$) as well. For non-equilibrium processes, heat is produced and the inequality sign in Eqn. (10.17) holds. Thus, it came as a surprise to many researchers when Jarzynski (1997a, 1997b, 2006, 2008) and Crooks (1998, 1999) pointed out that one can also obtain ΔF from non-equilibrium processes, when one does not consider a single trajectory from i to f but carries out a sampling over such non-equilibrium trajectories instead:

$$\Delta F = -k_{\mathrm{B}} T \ln \overline{\left[\exp\left(-\frac{W}{k_{\mathrm{B}} T} \right) \right]}. \tag{10.18}$$

Here the overbar stands for the average over a large enough number of trajectories. For a stochastic time evolution, as provided by Monte Carlo, it suffices that for the whole non-equilibrium process the transition probabilities between the microstates $\vec{X}$, $\vec{X}'$ still obey detailed balance,

$$\frac{W(\vec{X} \to \vec{X}'; \lambda)}{W(\vec{X}' \to \vec{X}; \lambda)} = \frac{\exp[-\mathcal{H}(\vec{X}; \lambda)/k_B T]}{\exp[-\mathcal{H}(\vec{X}'; \lambda)/k_B T]}. \tag{10.19}$$

Here it is understood that as the system evolves the work parameter is also updated, which explicitly means for the 'forward process'

$$(\vec{X}_n, \lambda_n) \to (\vec{X}_n, \lambda_{n+1}) \to (\vec{X}_{n+1}, \lambda_{n+1}), \tag{10.20}$$

initial conditions being sampled from the equilibrium distribution at λ_i. For the backward process, initial conditions are sampled from the equilibrium distribution at λ_f and transitions are carried out as follows:

$$(\vec{X}_n, \lambda_n) \to (\vec{X}_{n+1}, \lambda_n) \to (\vec{X}_{n+1}, \lambda_{n+1}), \tag{10.21}$$

where the states are labeled in reverse order, so that one starts at λ_f and ends at λ_i. The net change in the internal energy of the system, $\Delta E = \mathcal{H}(\vec{X}_f, \lambda_f) - \mathcal{H}(\vec{X}_i, \lambda_i)$, can be written as the sum of two terms, $\Delta E = W + Q$. Here

$$W = \sum_{n=1}^{f} [\mathcal{H}(\vec{X}_n, \lambda_{n+1}) - \mathcal{H}(\vec{X}_n, \lambda_n)]. \tag{10.22}$$

Changes of the energy due to changes of the work parameter are interpreted as the work performed on the system. These changes due to transitions from one point in phase space to the next at fixed λ,

$$Q = \sum_{n=1}^{f} [\mathcal{H}(\vec{X}_{n+1}, \lambda_{n+1}) - \mathcal{H}(\vec{X}_n, \lambda_{n+1})], \tag{10.23}$$

can be interpreted as the heat absorbed from the surroundings. The identity $\Delta E = W + Q$ is nothing but the first law of thermodynamics.

Apart from Eqn. (10.18) for the free energy difference, which is a statement relating to an average over the distribution $\rho(W)$ of the non-equilibrium work W (we can also rewrite Eqn. (10.18) as $F = -k_B T \ln \int dW \rho(W) \exp(-W/k_B T)$), we can also derive a symmetry relation (Crooks 1998, 1999)

$$\frac{\rho_F(+W)}{\rho_B(-W)} = \exp[(W - \Delta F)/k_B T], \tag{10.24}$$

where ρ_F, ρ_B stand for the distributions ρ describing the forward and backward process, Eqns. (10.20) and (10.21), respectively. Finally, we note that Eqn. (10.18) is not restricted to systems evolving by stochastic Monte Carlo dynamics but can also be derived for systems evolving via Newton's equation of motion (Jarzynski, 1997a, 1997b). In fact, within the context of 'steered Molecular Dynamics' simulation (Amaro and Luthey-Schulten, 2004), the method is most popular. However, care is needed, since sufficiently accurate results are obtained only if the distributions $\rho_F(W)$, $\rho_B(W)$ overlap strongly enough. In practice, it often turns out that best results are obtained when the increments $(\lambda_{n+1} - \lambda_n)$ are very small, so one is close to sampling an equilibrium path, and the method can be viewed as a variant of umbrella sampling. This problem of accuracy is also evident from applications of the technique to experimental studies on RNA molecules (Harris *et al.*, 2007).

10.11 OUTLOOK: VARIATIONS ON A THEME

In this chapter we have only mentioned a small fraction of the problems that have been considered in the literature. There are many related problems of non-equilibrium growth phenomena for which Monte Carlo simulation is an extremely useful tool. In this regard, we wish to cite just one more example, that of random sequential adsorption (e.g. Evans, 1993): consider the growth of coverage of a monolayer formed by dimers (or n-mers) which are randomly adsorbed but which obey excluded volume constraints. A special 'jamming coverage' then appears where further adsorption becomes impossible. Near this jamming coverage, slow dynamics is observed. This simple model and its extensions form another rich area for investigation that we have not really examined here.

REFERENCES

Alberts, B. (1994) *Molecular Biology of the Cell* (Garland, New York).

Amaro, R. and Luthey-Schulten, Z. (2004), *Chem. Phys.* **307**, 147.

Barabási, A.-L. and Stanley, H. E. (1995), *Fractal Concepts in Surface Growth* (Cambridge University Press, Cambridge).

Binder, K. and Stauffer, D. (1974), *Phys. Rev. Lett.* **33**, 1006.
Binder, K. and Stauffer, D. (1976), *Adv. Phys.* **25**, 343.
Binder, K. and Wang, J. S. (1989), *J. Stat. Phys.* **55**, 87.
Bolhuis, P. G., Dellago, C., Chandler, D., and Geissler, P. L. (2002), *Ann. Rev. Phys. Chem.* **59**, 291.
Bray, A. (1994), *Adv. Phys.* **43**, 357.
Caracciolo, S., Gambassi, A., Gubinelli, M., and Pelissetto, A. (2004), *J. Stat. Phys.* **115**, 281.
Chhabra, A., Matthews-Morgan, D., and Landau, D. P. (1986), *Phys. Rev. B* **34**, 4796.
Cirillo, E. N. M., Gonnella, G., and Saracco, G. P. (2005), *Phys. Rev. E* **72**, 026139.
Crooks, G. E. (1998), *J. Stat. Phys.* **90**, 1481.
Crooks, G. E. (1999), *Phys. Rev. E* **60**, 2721.
Dellago, C., Bolhuis, P. G., and Geissler, P. L. (2001), *Advances in Chemical Physics* (Wiley, New York).
Derks, D., Aarts, D. G. A. L., Bonn, D., Lekkerkerker, H. N. W., and Imhof, A. (2006). *Phys. Rev. Lett.* **97**, 038301.
Dubbeldam, J. L. A., Milchev, A., Rostashvili, V. G., and Vilgis, T. A., (2007), *Europhys. Lett.* **79**, 18002.
Eden, M. (1961), in *Proc. 4th Berkeley Symposium on Mathematical Statistics and Probability, Vol. IV*, ed. J. Neyman (University of California, Berkeley) p. 223.
Edwards, S. F. and Wilkinson, D. R. (1982), *Proc. R. Soc. A* **381**, 17.
Evans, J. W. (1993), *Rev. Mod. Phys.* **65**, 1281.
Family, F. and Landau, D. P. (1984), *Kinetics of Aggregation and Gelation* (North Holland, Amsterdam).
Farkas, Z., Derenyi, I., and Vicsek, T. (2003), *J. Phys.: Cond. Matter* **15**, S 1767.
Feder, J. (1988), *Fractals* (Plenum Press, New York).
Gilmer, G. H. and Broughton, J. Q. (1983), *J. Vac. Sci. Technol.* **B** 1, 298.
Gilmer, G. H., Leamy, H. J., and Jackson, K. A. (1974), *J. Cryst. Growth* **24/25**, 495.
Grest, G. S. and Srolovitz, D. J. (1985), *Phys. Rev. B* **32**, 3014.
Gunton, J. D., Gawlinski, E., and Kaski, K. (1988), *Dynamics of Ordering Processes in Condensed Matter*, eds. S. Komura and H. Furukawa (Plenum, New York), p. 101.
Han, J., Turner, S. W., and Craigherd, H. G. (1999), *Phys. Rev. Lett.* **83**, 1688.
Hanss, B., Leal-Pinto, E., Bruggeman, I. A., Copland, T. D., and Klotman, P. E. (1998), *Proc. Natl Acad. Sci. USA* **95**, 1921.
Harris, N. C., Song, Y., and Kiang, C. H. (2007), *Phys. Rev. Lett.* **99**, 068101.
Herrmann, H. J. (1986a), *Physics Reports* **136**, 153.
Herrmann, H. J. (1986b), *J. Stat. Phys.* **45**, 145.
Herrmann, H. J. (1992), in *The Monte Carlo Method in Condensed Matter Physics*, ed. K. Binder (Springer, Berlin).
Herrmann, H. J., Stauffer, D., and Landau, D. P. (1983), *J. Phys. A* **16**, 1221.
Janssen, H. K. and Schmittmann, B. (1986), *Z. Phys. B* **64**, 503.
Jarzynski, C. (1997a), *Phys. Rev. Lett.* **78**, 2690
Jarzynski, C. (1997b), *Phys. Rev. E* **56**, 5018.
Jarzynski, C. (2006), *Phys. Rev. E* **73**, 046105.
Jarzynski, C. (2008), *Eur. Phys. J. B* **64**, 331.
Jullien, R., Kolb, M., and Botet, R. (1984), in *Kinetics of Aggregation and Gelation*, eds. F. Family and D. P. Landau (North Holland, Amsterdam).
Kantor, Y. and Kardar, M. (2004), *Phys. Rev. E* **69**, 021806.
Kardar, M., Parisi, G., and Zhang, Y.-C. (1986), *Phys. Rev. Lett.* **56**, 889.

Kashchiev, D., van der Eerden, J. P., and van Leeuwen, C. (1997), *J. Cryst. Growth* **40**, 47.
Katz, S., Lebowitz, J. L., and Spohn, H. (1984), *Phys. Rev. B* **28**, 1655.
Komura, S. and Furukawa, H. (1988), *Dynamics of Ordering Processes in Condensed Matter Theory* (Plenum, New York).
Kremer, K. and Binder, K. (1984), *J. Chem. Phys*. **81**, 6381.
Kwak, W., Landau, D. P., and Schmittmann, B. (2004), *Phys. Rev. E* **69**, 066134.
Landau, D. P. and Pal, S. (1996), *Thin Solid Films* **272**, 184.
Leung, K.-T. (1991), *Phys. Rev. Lett*. **66**, 453.
Leung, K.-T. and Cardy, J. L. (1986), *J. Stat. Phys*. **44**, 567; erratum (1986), *J. Stat. Phys*. 45, 1087.
Måløy, K. J., Feder, J., and Jøssang, T. (1985), *Phys. Rev. Lett*. **55**, 2688.
Manneville, P. and de Seze, L. (1981), in *Numerical Methods in the Study of Critical Phenomena*, eds. I. Della Dora, J. Demongeot, and B. Lacolle (Springer, Berlin).
Marro, J. (2008), *Comp. Phys. Commun*. **179**, 144.
Meller, A. (2003), *J. Phys.: Condens. Matter* **15**, R581.
Meller, A., Nivon, L., and Branton, D. (2001), *Phys. Rev. Lett*. **86**, 3435.
Milchev, A., Binder, K., and Bhattacharya, A. (2004), *J. Chem. Phys*. **121**, 6042.
Milchev, A., Binder, K., and Heermann, D. W. (1986), *Z. Phys. B* **63**, 521.
Mitchell, S. J. and Landau, D. P. (2006), *Phys. Rev. Lett*. **97**, 025701.
Mouritsen, O. G. (1990), in *Kinetics of Ordering and Growth at Surfaces*, ed. M. G. Lagally (Plenum Press, New York), p. 1.
Muthukumar, M. (1999), *J. Chem. Phys*. **111**, 10379.
Onuki, A. (2002), *Phase Transition Dynamics* (Cambridge University Press, Cambridge).
Pal, S. and Landau, D. P. (1994), *Phys. Rev. B* **49**, 10, 597.
Pal, S. and Landau, D. P. (1999), *Physica A* **267**, 406.
Pal, S., Landau, D. P., and Binder, K. (2003), *Phys. Rev. E* **68**, 021601.
Panja, D., Barkema, G. T., and Kolomeisky, A. B. (2013), *J.Phys.: Condens. Matter* **25**, 413101.
Park, P. J. and Sung, W. (1998), *J. Chem. Phys.* **108**, 3013.
Praestgaard, E. L., Schmittmann, B., and Zia, R. K. P. (2000), *Eur. Phys. J. B* **18**, 675.
Sadiq, A. and Binder, K. (1984), *J. Stat. Phys*. **35**, 517.
Schmittmann, B. and Zia, R. K. P. (1995), in *Phase Transitions and Critical Phenomena*, vol. 17 (Academic Press, London), p. 1.
Smith, T. H., Vasilyev, O., Abraham, D. B., Maciolek, A., and Schmitt, M. (2008), *Phys. Rev. Lett*. **101**, 067203.
Stauffer, D. (1987), *Phil. Mag. B* **56**, 901.
Stauffer, D. (1997), *Int. J. Mod. Phys. C* **8**, 1263.
Sung, W. and Park, P. J. (1996), *Phys. Rev. Lett*. **77**, 783.
Swendsen, R. H., Kortman, P. J., Landau, D. P., and Müller-Krumbhaar, H. (1976), *J. Cryst. Growth* **35**, 73.
Toxvaerd, S. (1995), in *25 Years of Nonequilibrium Statistical Mechanics*, eds. J. J. Brey, J. Marro, J. M. Rubi, and M. San Miguel (Springer, Berlin), p. 338.
Tringides, M. C., Wu, P. K., and Lagally, M. G. (1987), *Phys. Rev. Lett*. **59**, 315.
Uebing, C. and Gomer, R. (1991), *J. Chem. Phys*. **95**, 7626, 7636, 7641, 7648.
Uebing, C. and Gomer, R. (1994), *Surf. Sci*. **306**, 419.
Van den Eijnden E. (2006), in *Computer Simulations in Condensed Matter: From Materials to Chemical Biology*, eds. M. Ferrario, G. Ciccotti, and K. Binder

(Springer, Heidelberg), vol. 1, p. 453.
Vicsek, T. and Family, F. (1985), *J. Phys. A* **18**, L75.
Vocks, H., Panja, D., Barkema, G. T., and Ball, R. C. (2008), *J. Phys.: Condens. Matter* **20**, 095224.
Wang, J.-S. (1996), *J. Stat. Phys.* **82**, 1409.
Witten, T. A. and Sander, L. M. (1981), *Phys. Rev. Lett.* **47**, 1400.
Wolf, D. E. and Villain, J. (1990), *Europhys. Lett.* **13**, 389.